

Faraday rotation spectrum of magneto-optical nanoparticle aggregates

Mahdiyeh Sadrara

Department of Physics, Kharazmi University, P.O. Box 15719-14911, Tehran, Iran

MirFaez Miri*

Department of Physics, University of Tehran, P.O. Box 14395-547, Tehran, Iran

(Received 2 July 2017; revised manuscript received 30 August 2017; published 19 September 2017)

The interaction of light with a cluster of gyrotropic spherical particles is studied in view of a miniaturized Faraday rotator. The electromagnetic fields are expanded in terms of the vector multipole fields and the expansion of the scattered field is related to that of the incident field. An incident linearly polarized light with polarization azimuth ψ becomes elliptically polarized upon scattering from the cluster. The polarization azimuth rotation and ellipticity angle variation are almost sinusoidal functions of 2ψ . With planar disordered clusters of bismuth-substituted yttrium iron garnet nanoparticles of radius 50 nm, polarization rotations about $\pm 4^\circ$ are achievable.

DOI: [10.1103/PhysRevB.96.115436](https://doi.org/10.1103/PhysRevB.96.115436)**I. INTRODUCTION**

In 1845 Faraday discovered that a magnetic field affects the propagation of light in a block of flint glass. He observed rotation of the plane of polarization of a linearly polarized light passing through glass along the magnetic field. Unlike optical activity, Faraday rotation is a nonreciprocal effect. Indeed optically active and magneto-optical media rotate the polarization relative to the direction of the wave vector and the magnetic field, respectively. Since Faraday's discovery, many researches have been devoted to magneto-optics [1–5]. A wide number of magneto-optical materials are thoroughly studied, including bismuth-, cerium-, lead-, and cobalt-substituted yttrium iron garnets [3]. Now bulk magneto-optical isolators, circulators, deflectors, intensity modulators, and bistable optical switches are of wide application [3]. Thin magneto-optical films are used to develop eddy-current imaging devices to detect cracks, flux-penetration imaging in high-temperature superconductors, current sensors, and magnetometers, to name a few [4]. Magneto-optical waveguides are employed to realize integrated nonreciprocal devices [5].

The polarization of light can be utilized as an information carrier in optical communications, sensing, and imaging. For these applications, there is a strong trend towards downsized optical components that manipulate the polarization of light. Most waveguide-type isolators and circulators are based on thin films of iron garnet grown on gadolinium gallium garnet substrate [5]. But in integrated optics technologies, common substrates are III–V semiconductors, silica, and silicon. To overcome such limitations, embedding magneto-optical *nanoparticles* in a matrix has gained attention. Composites containing γ -Fe₂O₃, Fe₃O₄, Co, Fe, Ni, and bismuth-substituted yttrium iron garnet (Bi:YIG) nanoparticles are studied [6–13].

It is now known that optical properties of nanoscopic materials differ from their bulk counterparts. Quite surprisingly, even at low fields ($<10^4$ G), gold nanoparticles do exhibit sizable magneto-optical response [14]. This effect is due to an increase of the magnetic Lorentz force induced by

the collective motion of the conduction electrons when the surface plasmon resonance is excited [14]. Magnetoplasmonic nanostructures composed of ferromagnets and noble metals are also promising [15]: The metallic constituent sustains surface plasmons, thus enhancing electromagnetic fields inside the ferromagnetic constituent which exhibits the magneto-optical response. Along this line of thought, core-shell Co-Ag, Fe-Ag, Au-coated Fe₂O₃ nanoparticles, and dumbbell-like Ag-CoFe₂O₄ nanoparticle pairs are studied [16–20].

The Mie theory for wave scattering from one isotropic particle is extended to the case of *one* gyrotropic particle [21–23]. But this does not immediately shed light on the properties of periodic arrays, random gases, and fractal clusters of nanoparticles. The coupled-dipole equations provide a picture of wave interaction with a populous cluster: Each particle behaves as a point dipole. The local field acting on any dipole is a superposition of the incident field and secondary fields produced by other dipoles. Since dipole-dipole interactions depend on the positions of particles, the geometrical characters of the cluster affect its optical response. Within the dipole approximation, the magneto-optical response of gold and silver nanoparticle aggregates are studied [24,25]. However, the dipole approximation is not reliable when the particles are too close. Using an extension of the layer-multiple-scattering method, *periodic* structures of gyrotropic particles are studied [26–30]. This rigorous full electrodynamic calculation takes advantage of the Bloch theorem; thus it is not applicable to the disordered and fractal aggregates.

In this paper, we study the interaction of light with an aggregate of gyrotropic spherical particles, in view of application as a miniaturized Faraday rotator. We present a multiparticle Mie theory applicable to ordered, disordered, and fractal aggregates. We expand all electromagnetic fields in terms of the vector multipole fields [31] and relate the expansion of the scattered field to that of the incident field. We consider linear, rectangular, and disordered clusters of Bi:YIG nanoparticles (see Fig. 1). Here the gap between neighbor particles may be even smaller than the radius of the particles. The incident linearly polarized light is specified by the polarization azimuth ψ . Using the azimuth χ and ellipticity angle β to characterize the vibration ellipse of the scattered field, we find that the polarization azimuth rotation $\chi - \psi$ and

*mirfaez_miri@ut.ac.ir

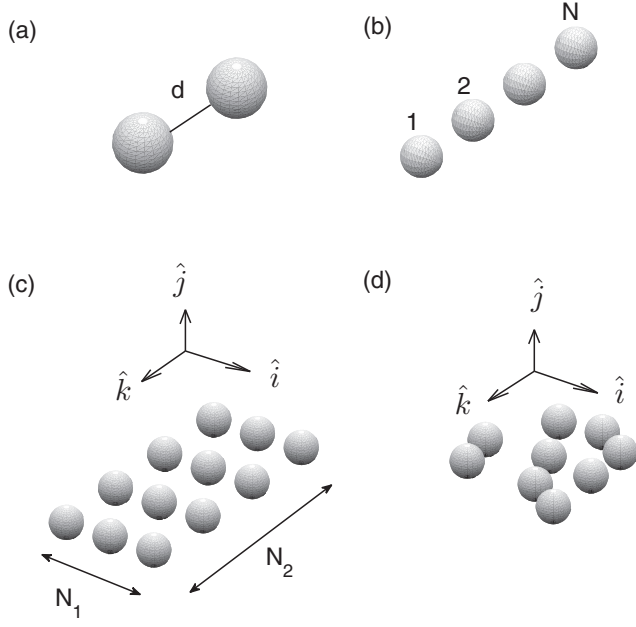


FIG. 1. Schematics of (a) a dimer, (b) a linear cluster, (c) a rectangular array, and (d) a disordered cluster of particles.

ellipticity angle variation β are almost sinusoidal functions of 2ψ :

$$\begin{aligned}\chi - \psi &\approx \chi_{\text{aniso}} \sin(2\psi - 2\psi_0) + \chi_{\text{gyro}}, \\ \beta &\approx \beta_{\text{aniso}} \sin(2\psi - 2\psi'_0) + \beta_{\text{gyro}},\end{aligned}\quad (1)$$

where χ_{aniso} , χ_{gyro} , β_{aniso} , and β_{gyro} depend on the composition, radius, and arrangement of particles, host medium dielectric constant, and light wavelength. For an ordered linear cluster, we find that $\chi_{\text{aniso}} = \beta_{\text{aniso}} = 0$ when the light wave vector, gyration vector, and cluster axis are parallel. For rectangular and disordered clusters, we find that $\chi_{\text{gyro}} \neq 0$ and $\beta_{\text{gyro}} \neq 0$. Quite remarkably, $\chi - \psi$ and β of a disordered cluster may be larger than that of a rectangular cluster. This facilitates the design of small polarization rotators. We remind that in the case of a *bulk* gyrotropic medium, the azimuth rotation and ellipticity angle variation are almost sinusoidal functions of 2ψ . The amplitudes χ_{aniso} and β_{aniso} , and the offsets χ_{gyro} and β_{gyro} , are largely controlled by the anisotropy and gyrotropy of the bulk medium, respectively [32]. Interestingly, nanoparticle aggregates also obey expression (1).

Our multiparticle Mie theory can be used to study other optical properties of a gyrotropic nanoparticle aggregate. In particular, absorption, linear dichroism, and circular dichroism spectra of the cluster are easily accessible. We briefly discuss the circular dichroism spectrum of linear clusters.

II. THEORY

We study the interaction of light with a cluster composed of N identical gyrotropic spherical particles (see Fig. 1). The radius a and position \mathbf{R}_α of the α th particle characterize the geometric properties of the cluster. We assume that the gyration vector of each particle is along the z axis. The electric permittivity tensor and the magnetic permeability of particles

are

$$\vec{\epsilon}_g = \epsilon_z \begin{pmatrix} \epsilon_r & -i\epsilon_k & 0 \\ i\epsilon_k & \epsilon_r & 0 \\ 0 & 0 & 1 \end{pmatrix}\quad (2)$$

and μ_g , respectively. The electric permittivity and the magnetic permeability of the host medium are ϵ_h and μ_h , respectively.

We assume that all the fields depend on time through $e^{-i\omega t}$. We denote the polarization vector and the wave vector of the incident plane wave by $\hat{\mathbf{u}}_{I\eta}$ ($\eta = 1, 2$) and $\hat{\mathbf{k}}_I$, respectively. We use $\hat{\mathbf{u}}_{S\eta}$ ($\eta = 1, 2$) and $\hat{\mathbf{k}}_S$ to characterize the scattered field. We denote an incident (scattered) field polarized along $\hat{\mathbf{u}}_{I\eta}$ ($\hat{\mathbf{u}}_{S\eta}$) by $\mathbf{E}_{I\eta}$ ($\mathbf{E}_{S\eta}$).

A. The electromagnetic fields inside a gyrotropic sphere

First we consider *one* gyrotropic sphere located at the center of coordinates. The fields inside the sphere obey the constitutive equations $\mathbf{D}_T(\mathbf{r}) = \vec{\epsilon}_g \mathbf{E}_T(\mathbf{r})$ and $\mathbf{B}_T(\mathbf{r}) = \mu_g \mathbf{H}_T(\mathbf{r})$, and the Maxwell equations

$$\nabla \cdot \mathbf{D}_T(\mathbf{r}) = 0, \quad (3)$$

$$\nabla \times \mathbf{E}_T(\mathbf{r}) = i \frac{\omega}{c} \mathbf{B}_T(\mathbf{r}), \quad (4)$$

$$\nabla \cdot \mathbf{B}_T(\mathbf{r}) = 0, \quad (5)$$

$$\nabla \times \mathbf{H}_T(\mathbf{r}) = -i \frac{\omega}{c} \mathbf{D}_T(\mathbf{r}), \quad (6)$$

where c is the velocity of light in vacuum. It turns out that \mathbf{D}_T satisfies the wave equation

$$\nabla \times \nabla \times [\epsilon_z \vec{\epsilon}_g^{-1} \mathbf{D}_T(\mathbf{r})] - k_g^2 \mathbf{D}_T(\mathbf{r}) = 0, \quad (7)$$

where $k_g^2 = \frac{\omega^2}{c^2} \mu_g \epsilon_z$.

The solution of the wave equation (7) can be expanded in terms of the vector multipole fields whose properties are summarized in Appendix A:

$$\mathbf{D}_T(\mathbf{r}) = \frac{k_{\text{in}}^2}{k_g^2} \sum_{lm} [C_{lm}^{(1)} \mathbf{J}_{lm}^{(1)}(\mathbf{r}, k_{\text{in}}) + C_{lm}^{(2)} \mathbf{J}_{lm}^{(2)}(\mathbf{r}, k_{\text{in}})]. \quad (8)$$

Note that the absence of \mathbf{L}_{lm} in the above expansion is enforced by the Maxwell equation (3). It can be shown that

$$\epsilon_z \vec{\epsilon}_g^{-1} \cdot \mathbf{J}_{lm}^{(1)} = \sum_{qp} (\tilde{g}_{qp}^{lm} \mathbf{J}_{qp}^{(1)} + \tilde{e}_{qp}^{lm} \mathbf{J}_{qp}^{(2)} + \tilde{f}_{qp}^{lm} \mathbf{L}_{qp}), \quad (9)$$

$$\epsilon_z \vec{\epsilon}_g^{-1} \cdot \mathbf{J}_{lm}^{(2)} = \sum_{qp} (\tilde{g}_{qp}^{lm} \mathbf{J}_{qp}^{(1)} + \tilde{e}_{qp}^{lm} \mathbf{J}_{qp}^{(2)} + \tilde{f}_{qp}^{lm} \mathbf{L}_{qp}). \quad (10)$$

Explicit expressions for the coefficients \tilde{g}_{qp}^{lm} , \tilde{e}_{qp}^{lm} , \tilde{f}_{qp}^{lm} , \tilde{g}_{qp}^{lm} , \tilde{e}_{qp}^{lm} , and \tilde{f}_{qp}^{lm} are in Appendix B. It follows from Eqs. (7)–(10) that

$$\begin{aligned} \sum_{lm'l'm'} \left[C_{l'm'}^{(1)} \tilde{g}_{lm}^{l'm'} + C_{l'm'}^{(2)} \tilde{g}_{lm}^{l'm'} - \frac{k_g^2}{k_{\text{in}}^2} C_{lm}^{(1)} \right] \mathbf{J}_{lm}^{(1)}(\mathbf{r}, k_{\text{in}}) \\ + \left[C_{l'm'}^{(1)} \tilde{e}_{lm}^{l'm'} + C_{l'm'}^{(2)} \tilde{e}_{lm}^{l'm'} - \frac{k_g^2}{k_{\text{in}}^2} C_{lm}^{(2)} \right] \mathbf{J}_{lm}^{(2)}(\mathbf{r}, k_{\text{in}}) = 0. \end{aligned}$$

Thus the coefficients $C_{l'm'}^{(p)}$ and the wave number k_{in} can be determined from the following eigenvalue problem:

$$\sum_{p'l'm'} S_{plm;p'l'm'} C_{l'm'}^{(p)} = \frac{k_g^2}{k_{\text{in}}^2} C_{l'm'}^{(p)} \quad (p, p' = 1, 2), \quad (11)$$

where $S_{1lm;1l'm'} = \tilde{g}_{lm}^{l'm'}$, $S_{1lm;2l'm'} = \tilde{g}_{lm}^{l'm'}$, $S_{2lm;1l'm'} = \tilde{e}_{lm}^{l'm'}$, and $S_{2lm;2l'm'} = \tilde{e}_{lm}^{l'm'}$. We perform multipole expansions of the fields up to a multipole order l_{max} to guarantee the numerical stability of the calculation. We use the subscript $j = 1, 2, \dots, 2l_{\text{max}}(l_{\text{max}} + 2)$ to enumerate the eigenvalues and eigenvectors of the matrix \mathbf{S} . The general solution of the wave equation (7) is

$$\mathbf{D}_{\mathbf{T}}(\mathbf{r}) = \sum_j b_j \frac{k_j^2}{k_g^2} \sum_{lm} [C_{lm;j}^{(1)} \mathbf{J}_{lm}^{(1)}(\mathbf{r}, k_j) + C_{lm;j}^{(2)} \mathbf{J}_{lm}^{(2)}(\mathbf{r}, k_j)], \quad (12)$$

where the coefficients b_j are determined by the boundary conditions.

B. Scattering of electromagnetic waves by a cluster of gyrotropic particles

It is wise to expand the incident field $\mathbf{E}_{I\eta} = E_0 \hat{\mathbf{u}}_{I\eta} e^{i\mathbf{k}\cdot\mathbf{r}}$ and the scattered field $\mathbf{E}_{S\eta}$ in terms of the vector multipole fields:

$$\begin{aligned} \mathbf{E}_{I\eta} &= E_0 \sum_{plm} \mathbf{J}_{lm}^{(p)}(\mathbf{r}, k) W_{I\eta lm}^{(p)}, \\ \mathbf{E}_{S\eta} &= E_0 \sum_{\alpha} \sum_{plm} \mathbf{H}_{lm}^{(p)}(\mathbf{r}_{\alpha}, k) \mathcal{A}_{\eta\alpha lm}^{(p)}, \end{aligned} \quad (13)$$

where $W_{I\eta lm}^{(p)} \equiv W_{lm}^{(p)}(\hat{\mathbf{u}}_{I\eta}, \hat{\mathbf{k}}_l)$, $\mathbf{r}_{\alpha} = \mathbf{r} - \mathbf{R}_{\alpha}$, $k = \frac{\omega}{c} \sqrt{\mu_h \epsilon_h}$, and $p = 1, 2$. Indeed $W_{lm}^{(p)}(\hat{\mathbf{e}}, \hat{\mathbf{k}}) = 4\pi i^{p+1} \hat{\mathbf{e}} \cdot \mathbf{Z}_{lm}^{(p)*}(\hat{\mathbf{k}})$. The properties of transverse vector harmonics $\mathbf{Z}_{lm}^{(p)}$ are summarized in Appendix A. In Eq. (13) the scattered field is a sum of multipole fields with different origins, whereas the incident field is a sum of multipole fields centered at $\mathbf{R}_0 = 0$. Using the celebrated addition theorem, all fields can be rewritten in terms of multipole fields centered at \mathbf{R}_{α} :

$$\begin{aligned} \mathbf{E}_{I\eta} &= E_0 \sum_{plm} \sum_{p'l'm'} \mathbf{J}_{lm}^{(p)}(\mathbf{r}_{\alpha}, k) \mathcal{J}_{\alpha lm 0l'm'}^{(pp')} W_{I\eta l'm'}^{(p')}, \quad (14) \\ \mathbf{E}_{S\eta} &= E_0 \sum_{plm} \left[\mathbf{H}_{lm}^{(p)}(\mathbf{r}_{\alpha}, k) \mathcal{A}_{\eta\alpha lm}^{(p)} \right. \\ &\quad \left. + \sum_{\alpha' p'l'm'} \mathbf{J}_{lm}^{(p)}(\mathbf{r}_{\alpha}, k) \mathcal{H}_{\alpha lm \alpha' l'm'}^{(pp')} \mathcal{A}_{\eta\alpha' l'm'}^{(p')} \right], \end{aligned} \quad (15)$$

where $\mathcal{H}_{\alpha lm \alpha' l'm'}^{(pp')}$ and $\mathcal{J}_{\alpha lm 0l'm'}^{(pp')}$ are given in Ref. [31]. The scattered field can also be written as $\mathbf{E}_{S\eta} = E_0 \sum_{plm} \mathbf{H}_{lm}^{(p)}(\mathbf{r}, k) \mathcal{A}_{\eta lm}^{(p)}$, where

$$\mathcal{A}_{\eta lm}^{(p)} = \sum_{\alpha'} \sum_{p'l'm'} \mathcal{J}_{0lm \alpha' l'm'}^{(pp')} \mathcal{A}_{\eta\alpha' l'm'}^{(p')}. \quad (16)$$

As clarified before, the electric displacement vector within the α th sphere is

$$\mathbf{D}_{\mathbf{T}} = \sum_j \frac{b_{\alpha j} k_j^2}{k_g^2} \sum_{lm} [C_{\eta lm;j}^{(1)} \mathbf{J}_{lm}^{(1)}(\mathbf{r}_{\alpha}, k_j) + C_{\eta lm;j}^{(2)} \mathbf{J}_{lm}^{(2)}(\mathbf{r}_{\alpha}, k_j)]. \quad (17)$$

Using Eqs. (9)–(11) it is straightforward to write the electric field as

$$\begin{aligned} \mathbf{E}_{\mathbf{T}} &= \overset{\leftarrow}{\epsilon}_g^{-1} \cdot \mathbf{D}_{\mathbf{T}} \\ &= \sum_j b_{\alpha j} \left\{ \frac{k_j^2 \omega_{\eta 00;j}}{k_g^2} \mathbf{L}_{00}(\mathbf{r}_{\alpha}, k_j) + \sum_{lm} \left[\frac{k_j^2 \omega_{\eta lm;j}}{k_g^2} \mathbf{L}_{lm}(\mathbf{r}_{\alpha}, k_j) \right. \right. \\ &\quad \left. \left. + C_{\eta lm;j}^{(1)} \mathbf{J}_{lm}^{(1)}(\mathbf{r}_{\alpha}, k_j) + C_{\eta lm;j}^{(2)} \mathbf{J}_{lm}^{(2)}(\mathbf{r}_{\alpha}, k_j) \right] \right\}, \end{aligned} \quad (18)$$

where $\omega_{\eta lm;j} = \sum_{l'm'} (C_{\eta l'm';j}^{(1)} \tilde{f}_{lm}^{l'm'} + C_{\eta l'm';j}^{(2)} \tilde{f}_{lm}^{l'm'})$ and $\omega_{\eta 00;j} = -\sqrt{2/3} \epsilon_k' C_{\eta 10;j}^{(1)} + i\sqrt{2/15} (\epsilon_r' - 1) C_{\eta 20;j}^{(2)}$. The Maxwell equation (4) and identities (A5) then imply that

$$\mathbf{H}_{\mathbf{T}} = \sum_{j,l,m} \frac{-ic b_{\alpha j} k_j}{\omega \mu_g} [C_{\eta lm;j}^{(1)} \mathbf{J}_{lm}^{(2)}(\mathbf{r}_{\alpha}, k_j) + C_{\eta lm;j}^{(2)} \mathbf{J}_{lm}^{(1)}(\mathbf{r}_{\alpha}, k_j)]. \quad (19)$$

The boundary conditions across the surface of the α th sphere can be written as

$$\int (\mathbf{H}_{I\eta} + \mathbf{H}_{S\eta}) \cdot \mathbf{Z}_{lm}^{(p)*} d\Omega = \int \mathbf{H}_{T\eta} \cdot \mathbf{Z}_{lm}^{(p)*} d\Omega, \quad (20)$$

$$\int (\mathbf{E}_{I\eta} + \mathbf{E}_{S\eta}) \cdot \mathbf{Z}_{lm}^{(p)*} d\Omega = \int \mathbf{E}_{T\eta} \cdot \mathbf{Z}_{lm}^{(p)*} d\Omega, \quad (21)$$

where $p = 1, 2$. The multipole expansion of the fields and identities (A7) then yield

$$\begin{aligned} \mathcal{W}_{I\eta\alpha lm}^{(1)} &= -\frac{h_l(x)}{j_l(x)} \mathcal{A}_{\eta\alpha lm}^{(1)} - \sum_{\alpha' p'l'm'} \mathcal{H}_{\alpha lm \alpha' l'm'}^{(1p')} \mathcal{A}_{\eta\alpha' l'm'}^{(p')} \\ &\quad + \sum_j b_{\alpha j} \frac{j_l(x_j)}{j_l(x)} C_{\eta lm;j}^{(1)}, \end{aligned} \quad (22)$$

$$\begin{aligned} \mathcal{W}_{I\eta\alpha lm}^{(2)} &= -\frac{h_l(x)}{j_l(x)} \mathcal{A}_{\eta\alpha lm}^{(2)} - \sum_{\alpha' p'l'm'} \mathcal{H}_{\alpha lm \alpha' l'm'}^{(2p')} \mathcal{A}_{\eta\alpha' l'm'}^{(p')} \\ &\quad + \frac{\mu_h}{\mu_g} \sum_j \frac{b_{\alpha j} k_j}{k} \frac{j_l(x_j)}{j_l(x)} C_{\eta lm;j}^{(2)}, \end{aligned} \quad (23)$$

$$\begin{aligned} \mathcal{W}_{I\eta\alpha lm}^{(1)} &= -\frac{[x h_l(x)]'}{[x j_l(x)]'} \mathcal{A}_{\eta\alpha lm}^{(1)} - \sum_{\alpha' p'l'm'} \mathcal{H}_{\alpha lm \alpha' l'm'}^{(1p')} \mathcal{A}_{\eta\alpha' l'm'}^{(p')} \\ &\quad + \frac{\mu_h}{\mu_g} \sum_j b_{\alpha j} \frac{[x_j j_l(x_j)]'}{[x j_l(x)]'} C_{\eta lm;j}^{(1)}, \end{aligned} \quad (24)$$

$$\begin{aligned} \mathcal{W}_{I\eta\alpha lm}^{(2)} &= -\frac{[x h_l(x)]'}{[x j_l(x)]'} \mathcal{A}_{\eta\alpha lm}^{(2)} - \sum_{\alpha' p'l'm'} \mathcal{H}_{\alpha lm \alpha' l'm'}^{(2p')} \mathcal{A}_{\eta\alpha' l'm'}^{(p')} \\ &\quad + \sum_j b_{\alpha j} \left[\frac{k [x_j j_l(x_j)]'}{k_j [x j_l(x)]'} C_{\eta lm;j}^{(2)} \right. \\ &\quad \left. - \frac{i\sqrt{l(l+1)} k k_j j_l(x_j)}{k_g^2 [x j_l(x)]'} \omega_{\eta lm;j} \right]. \end{aligned} \quad (25)$$

Here $\mathcal{W}_{l\eta\alpha lm}^{(p)} = \sum_{p'l'm'} \mathcal{J}_{alm0'l'm'}^{(pp')} \mathcal{W}_{l\eta l'm'}^{(p)}$, $x = ka$, and $x_j = k_j a$. The above equations suggest to define

$$\sigma_{l\eta\alpha lm}^{(p)} = \mathcal{W}_{l\eta\alpha lm}^{(p)} + \sum_{\alpha' p' l' m'} \mathcal{H}_{\alpha l m \alpha' l' m'}^{(pp')} \mathcal{A}_{\eta\alpha' l' m'}^{(p')}. \quad (26)$$

To represent Eqs. (22)–(25) in a more compact form, the following notations are used. Here $l = 1, 2, \dots, l_{\max}$ and $-l \leq m \leq l$. A combined index is $n = l(l+1) + m$, where $n = 1, 2, \dots, \bar{n} = l_{\max}(l_{\max} + 2)$. We let \mathcal{A} , \mathbf{b} , and $\boldsymbol{\sigma}$ denote column matrices. For example, $\mathcal{A} = [\mathcal{A}_{\alpha 1}]$, where $\mathcal{A}_{\alpha 1} = \begin{bmatrix} \mathcal{A}_{\alpha, \bar{n}+1} \\ \vdots \\ \mathcal{A}_{\alpha, \bar{n}} \end{bmatrix}$ and $\mathcal{A}_{\alpha 2} = \begin{bmatrix} \mathcal{A}_{\alpha, \bar{n}+1} \\ \vdots \\ \mathcal{A}_{\alpha, \bar{n}} \end{bmatrix}$. Indeed $\mathcal{A}_{\eta\alpha lm}^{(1)} \rightarrow \mathcal{A}_{\alpha 1}$ and $\mathcal{A}_{\eta\alpha lm}^{(2)} \rightarrow \mathcal{A}_{\alpha 2}$. We let $\mathbf{U} = \begin{bmatrix} U^{11} & U^{12} \\ U^{21} & U^{22} \end{bmatrix}$, $\mathbf{V} = \begin{bmatrix} V^{11} & V^{12} \\ V^{21} & V^{22} \end{bmatrix}$, $\boldsymbol{\Lambda} = \begin{bmatrix} \Lambda^{11} & \mathbf{0} \\ \mathbf{0} & \Lambda^{22} \end{bmatrix}$, and $\boldsymbol{\Theta} = \begin{bmatrix} \Theta^{11} & \mathbf{0} \\ \mathbf{0} & \Theta^{22} \end{bmatrix}$, where U^{11} , U^{12} , etc. are $\bar{n} \times \bar{n}$ matrices. Now Eqs. (22)–(25) can be written as

$$\begin{aligned} \boldsymbol{\Lambda} \mathcal{A} + \mathbf{U} \mathbf{b} &= \boldsymbol{\sigma}, \\ \boldsymbol{\Theta} \mathcal{A} + \mathbf{V} \mathbf{b} &= \boldsymbol{\sigma}. \end{aligned} \quad (27)$$

Here

$$\begin{aligned} \Lambda_{nn'}^{11} &= \Lambda_{nn'}^{22} = -\frac{h_l(x)}{j_l(x)} \delta_{nn'}, \\ \Theta_{nn'}^{11} &= \Theta_{nn'}^{22} = -\frac{[x h_l(x)]'}{[x j_l(x)]'} \delta_{nn'}, \\ U_{ni}^{11} &= \frac{j_l(x_i)}{j_l(x)} C_{\eta lm; i}^{(1)}, \\ U_{ni}^{12} &= \frac{j_l(x_{i+\bar{n}})}{j_l(x)} C_{\eta lm; i+\bar{n}}^{(1)}, \\ U_{ni}^{21} &= \frac{\mu_h k_i j_l(x_i)}{\mu_g k j_l(x)} C_{\eta lm; i}^{(2)}, \\ U_{ni}^{22} &= \frac{\mu_h k_{i+\bar{n}} j_l(x_{i+\bar{n}})}{\mu_g k j_l(x)} C_{\eta lm; i+\bar{n}}^{(2)}, \\ V_{ni}^{11} &= \frac{\mu_h [x_i j_l(x_i)]'}{\mu_g [x j_l(x)]'} C_{\eta lm; i}^{(1)}, \\ V_{ni}^{12} &= \frac{\mu_h [x_{i+\bar{n}} j_l(x_{i+\bar{n}})]'}{\mu_g [x j_l(x)]'} C_{\eta lm; i+\bar{n}}^{(1)}, \\ V_{ni}^{21} &= \frac{k [x_i j_l(x_i)]'}{k_i [x j_l(x)]'} C_{\eta lm; i}^{(2)} - \frac{i \sqrt{l(l+1)} k k_i j_l(x_i)}{k_g^2 [x j_l(x)]'} \omega_{\eta lm; i}, \\ V_{ni}^{22} &= \frac{k [x_{i+\bar{n}} j_l(x_{i+\bar{n}})]'}{k_{i+\bar{n}} [x j_l(x)]'} C_{\eta lm; i+\bar{n}}^{(2)} \\ &\quad - \frac{i \sqrt{l(l+1)} k k_{i+\bar{n}} j_l(x_{i+\bar{n}})}{k_g^2 [x j_l(x)]'} \omega_{\eta lm; i+\bar{n}}. \end{aligned} \quad (28)$$

Note that in the above equations $n = l(l+1) + m$ and $1 \leq i \leq \bar{n}$. Introducing the matrices

$$\begin{aligned} \mathbf{R} &= (\boldsymbol{\Lambda} \mathbf{V} - \boldsymbol{\Theta} \mathbf{U})^{-1} (\boldsymbol{\Lambda} - \boldsymbol{\Theta}), \\ \mathbf{T} &= \boldsymbol{\Theta}^{-1} - \boldsymbol{\Theta}^{-1} \mathbf{V} \mathbf{R}, \end{aligned} \quad (29)$$

the solution of the set of equations (27) can be written as $\mathbf{b} = \mathbf{R} \boldsymbol{\sigma}$ and $\mathcal{A} = \mathbf{T} \boldsymbol{\sigma}$. In other words,

$$\begin{aligned} \begin{bmatrix} \mathcal{A}_{\alpha 1} \\ \mathcal{A}_{\alpha 2} \end{bmatrix} &= \begin{bmatrix} T^{11} & T^{12} \\ T^{21} & T^{22} \end{bmatrix} \left\{ \begin{bmatrix} \mathcal{W}_{\alpha 1} \\ \mathcal{W}_{\alpha 2} \end{bmatrix} \right. \\ &\quad \left. + \sum_{\alpha'} \begin{bmatrix} \mathcal{H}^{11} & \mathcal{H}^{12} \\ \mathcal{H}^{21} & \mathcal{H}^{22} \end{bmatrix} \begin{bmatrix} \mathcal{A}_{\alpha' 1} \\ \mathcal{A}_{\alpha' 2} \end{bmatrix} \right\}, \end{aligned} \quad (30)$$

whose solution provides the amplitudes of the scattered fields.

III. NUMERICAL RESULTS

The scattering of electromagnetic waves from *one* gyrotropic sphere is studied in detail [21–23]. We reproduced some numerical results of Ref. [23] as a test of our code.

We study optical response of magnetically saturated Bi:YIG nanoparticles embedded in air. Indeed Bi:YIG nanoparticles have been synthesized by a variety of methods [11–13]. We obtain the dielectric tensor spectra of $Y_{3-x}Bi_xFe_5O_{12}$ with $x = 1.07$ from Doormann, Krumme, and Lenz [33].

We consider linear, rectangular, and disordered clusters of nanoparticles (see Fig. 1). We assume that the radius of particles is $a = 50$ nm. In linear clusters, the centers of adjacent particles are at a distance $2a + d$. The rectangular and disordered clusters, each composed of 64 particles, are in the xOz plane. The array has 16 rows and 4 columns. The columns (rows) of the rectangle are parallel to the \hat{z} (\hat{x}) axis. Two vectors $2.4a\hat{z}$ and $4.5a\hat{x}$ specify the rectangular unit cell. The particles of the disordered cluster are uniformly distributed in a square of length $27a$.

A. Rotation of light polarization plane

We assume that the cluster interacts with a linearly polarized light $\mathbf{E}_I = E_0(\cos \psi \hat{\mathbf{e}}_1 + \sin \psi \hat{\mathbf{e}}_2) e^{i\mathbf{k}_I \cdot \mathbf{r}}$. Here $\mathbf{k}_I = k \hat{\mathbf{k}}_I = k(\sin \theta \cos \phi, \sin \theta \sin \phi, \cos \theta)$ is the wave vector, and $\hat{\mathbf{e}}_1 = (\cos \theta \cos \phi, \cos \theta \sin \phi, -\sin \theta)$ and $\hat{\mathbf{e}}_2 = (-\sin \phi, \cos \phi, 0)$ are the polarization vectors. We calculate $\mathbf{E}_S = E_{S1} \hat{\mathbf{e}}_1 + E_{S2} \hat{\mathbf{e}}_2$, the electric field scattered by the cluster. In the far (radiation) zone

$$\begin{pmatrix} E_{S1} \\ E_{S2} \end{pmatrix} = \frac{E_0 e^{ikr}}{r} \begin{pmatrix} f_{11}(\hat{\mathbf{k}}_S, \hat{\mathbf{k}}_I) \cos \psi + f_{12}(\hat{\mathbf{k}}_S, \hat{\mathbf{k}}_I) \sin \psi \\ f_{21}(\hat{\mathbf{k}}_S, \hat{\mathbf{k}}_I) \cos \psi + f_{22}(\hat{\mathbf{k}}_S, \hat{\mathbf{k}}_I) \sin \psi \end{pmatrix}, \quad (31)$$

where the elements of the scattering amplitude matrix are [31]

$$f_{\eta' \eta} = \frac{-i}{4\pi k} \sum_{plm} W_{lm}^{(p)*}(\hat{\mathbf{u}}_{S\eta'}, \hat{\mathbf{k}}_S) A_{lm}^{(p)}(\hat{\mathbf{u}}_{I\eta}, \hat{\mathbf{k}}_I). \quad (32)$$

The scattered field is elliptically polarized. The vibration ellipse can be described by the azimuth χ , the angle between the semimajor axis and the unit vector $\hat{\mathbf{e}}_1$, and ellipticity $\tan \beta$, the ratio of the length of the semiminor axis to that of the semimajor axis. Indeed

$$\begin{aligned} \chi &= \frac{1}{2} \arctan \left(-\frac{U}{Q} \right), \\ \beta &= \frac{1}{2} \arcsin \left(-\frac{V}{I} \right), \end{aligned} \quad (33)$$

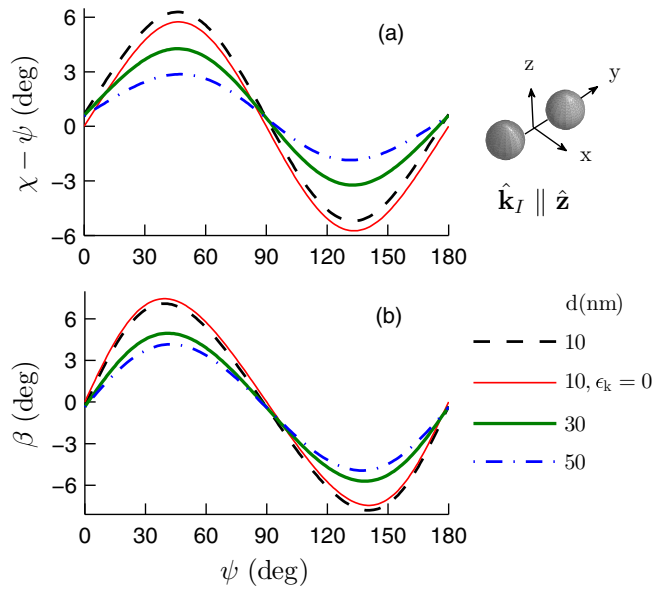


FIG. 2. (a) $\chi - \psi$ and (b) β as a function of ψ for a dimer of Bi:YIG nanoparticles. The dimer is along the \hat{y} axis, $a = 50$ nm, $\lambda = 365$ nm, $\hat{\mathbf{k}}_I \parallel \hat{\mathbf{z}}$, and $\hat{\mathbf{k}}_S \parallel \hat{\mathbf{z}}$.

where $I = |E_{S1}|^2 + |E_{S2}|^2$, $Q = |E_{S1}|^2 - |E_{S2}|^2$, $U = -2\text{Re}(E_{S1}E_{S2}^*)$, and $V = 2\text{Im}(E_{S1}E_{S2}^*)$ are the Stokes parameters [31,34]. The azimuth and the ellipticity angle of the incident wave are ψ and zero, respectively. The polarization azimuth rotation $\chi - \psi$ and the ellipticity angle variation β are of immediate interest.

Figure 2 shows $\chi - \psi$ and β as a function of ψ for a dimer of Bi:YIG nanoparticles. The dimer is along the \hat{y} axis; $\lambda = 365$ nm, and $\hat{\mathbf{k}}_I \parallel \hat{\mathbf{z}}$ and $\hat{\mathbf{k}}_S \parallel \hat{\mathbf{z}}$ are assumed. We find that $\chi - \psi$ and β are almost sinusoidal functions of 2ψ . For example, $\chi - \psi \approx 5.66^\circ \sin(2\psi + 1.02^\circ) + 0.55^\circ$ and $\beta \approx 7.37^\circ \sin(2\psi + 0.29^\circ) - 0.35^\circ$ when $d = 10$ nm. On increasing the gap d , the amplitudes of $\chi - \psi$ and β decrease. Even at $d = 50$ nm, maximum azimuth rotation 2.87° and maximum ellipticity angle variation 4.17° are considerable. But one must notice that $\chi - \psi$ and β are not completely due to the gyrotropy of particles. In the case of $d = 10$ nm, the results for gyrotropic particles with $\epsilon_k \neq 0$ and anisotropic particles with $\epsilon_k = 0$ are shown as dashed (black) and thin solid (red) lines, respectively. On introducing the gyrotropy, the maximum of $\chi - \psi$ and β change by 0.54° and -0.36° , respectively.

Figures 3(a)–3(f) show $\chi - \psi$ and β as a function of ψ for linear, rectangular, and disordered clusters composed of 64 Bi:YIG nanoparticles. The linear cluster is along the $\hat{\mathbf{z}}$

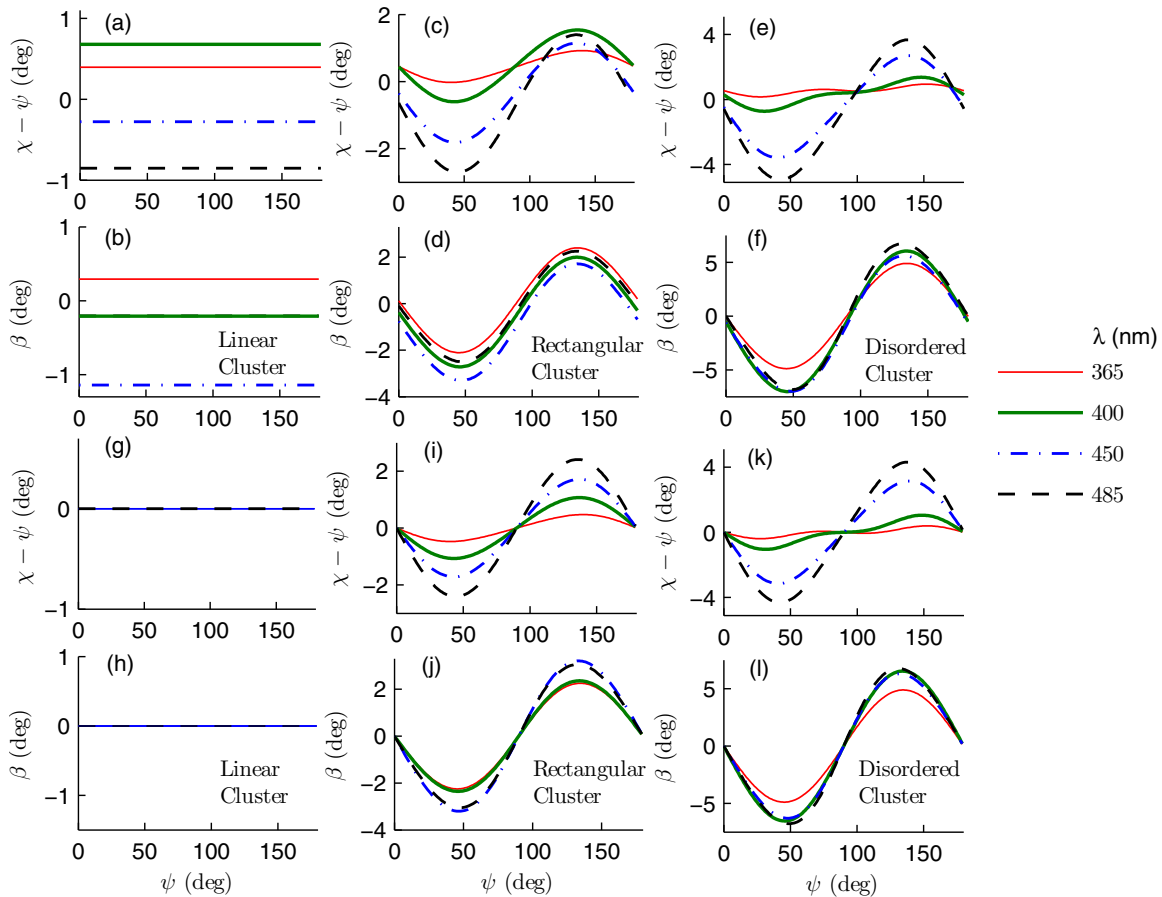


FIG. 3. (a) $\chi - \psi$ and (b) β versus ψ for a linear cluster. The cluster is along the $\hat{\mathbf{z}}$ axis. $d = 0.4a = 20$ nm. (c) $\chi - \psi$ and (d) β versus ψ for a rectangular cluster. (e) $\chi - \psi$ and (f) β versus ψ for a disordered cluster. The clusters are composed of 64 Bi:YIG nanoparticles of radius $a = 50$ nm. $\hat{\mathbf{k}}_I \parallel \hat{\mathbf{z}}$ and $\hat{\mathbf{k}}_S \parallel \hat{\mathbf{z}}$ are assumed. For clusters composed of anisotropic particles with $\epsilon_k = 0$, the corresponding plots are shown in (g)–(l).

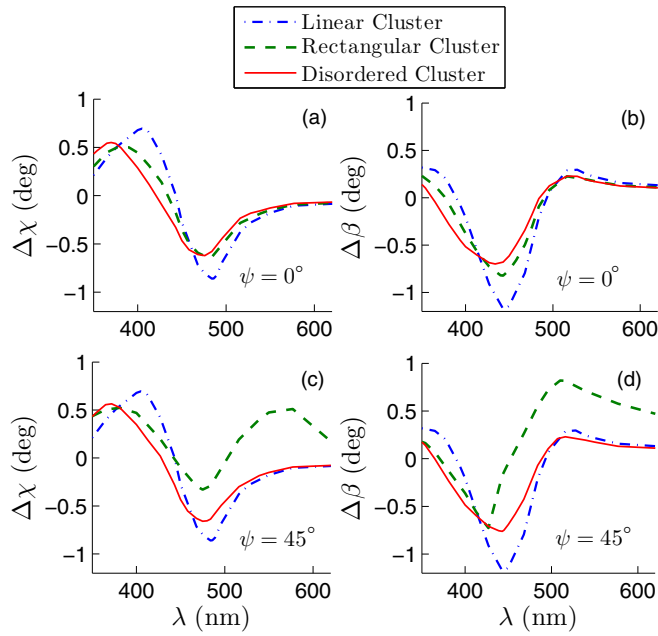


FIG. 4. (a) $\Delta\chi$ and (b) $\Delta\beta$ as a function of λ . Here $\psi = 0^\circ$. The plots corresponding to $\psi = 45^\circ$ are shown in (c) and (d), respectively. $\hat{\mathbf{k}}_I \parallel \hat{\mathbf{z}}$ and $\hat{\mathbf{k}}_S \parallel \hat{\mathbf{z}}$ are assumed.

axis. Here $d = 0.4a = 20$ nm, $\hat{\mathbf{k}}_I \parallel \hat{\mathbf{z}}$, and $\hat{\mathbf{k}}_S \parallel \hat{\mathbf{z}}$. We find that $\chi - \psi$ and β of a linear cluster are independent of ψ . $\chi - \psi$ and β exhibit both positive and negative values as the wavelength λ varies. For example, $\chi - \psi$ becomes $+0.68^\circ$ at wavelength 400 nm, and reaches -0.85° at wavelength 485 nm. β becomes $+0.29^\circ$ at wavelength 365 nm, and reaches -1.14° at wavelength 450 nm. In the case of rectangular and disordered clusters, $\chi - \psi$ and β are almost sinusoidal functions of 2ψ . Note that at $\psi = 0$ and wavelengths 365, 400, 450, and 485 nm, $\chi - \psi$ of a rectangular cluster are 0.45° , 0.45° , -0.35° , and -0.64° , respectively. Quite remarkably, the disordered cluster may offer large values of $\chi - \psi$ and β . For example, at wavelength 485 nm, the maximum $\chi - \psi$ of a disordered cluster is 3.68° , while that of a rectangular cluster is 1.40° . At wavelength 450 nm, the maximum β of a disordered cluster is 5.60° , while that of a rectangular cluster is 1.71° . Note that at $\psi = 0$ and wavelengths 365, 400, 450, and 485 nm, $\chi - \psi$ of a disordered cluster are 0.5431° , 0.2861° , -0.4653° , and -0.5775° , respectively. Figures 3(g)–3(i) show $\chi - \psi$ and β for clusters composed of anisotropic particles with $\epsilon_k = 0$. Here $\chi - \psi$ and β of a linear cluster are both zero. $\chi - \psi$ and β of rectangular and disordered clusters are almost sinusoidal functions of 2ψ , but with $\chi_{\text{gyro}} = \beta_{\text{gyro}} = \psi_0 = \psi'_0 = 0$ [see expression (1)].

To better see the influence of gyrotropy,

$$\begin{aligned} \Delta\chi &\equiv \chi(\epsilon_k) - \chi(\epsilon_k = 0), \\ \Delta\beta &\equiv \beta(\epsilon_k) - \beta(\epsilon_k = 0), \end{aligned} \quad (34)$$

are of use. Figure 4 shows $\Delta\chi$ and $\Delta\beta$ as a function of λ for linear, rectangular, and disordered clusters. Here $\hat{\mathbf{k}}_I \parallel \hat{\mathbf{z}}$ and $\hat{\mathbf{k}}_S \parallel \hat{\mathbf{z}}$. $\Delta\chi$ and $\Delta\beta$ of these three clusters have the same order of magnitude, whether $\psi = 0^\circ$ or $\psi = 45^\circ$. For a disordered cluster, the maximum and minimum of $\Delta\chi$ are 0.56° and

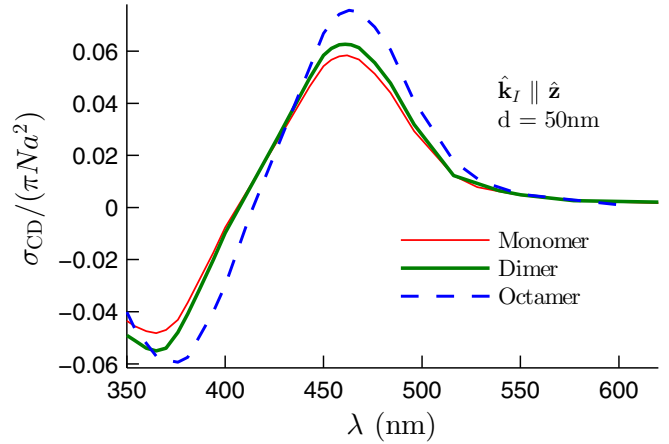


FIG. 5. $\sigma_{\text{CD}}/(\pi Na^2)$ for a monomer, dimer, and octamer of Bi:YIG nanoparticles. Here $a = d = 50$ nm and $\hat{\mathbf{k}}_I \parallel \hat{\mathbf{z}}$. The dimer and octamer are along the $\hat{\mathbf{z}}$ axis.

-0.62° when $\psi = 0^\circ$. The maximum and minimum of $\Delta\beta$ are 0.23° and -0.76° when $\psi = 45^\circ$. These examples show that, even in the case of disordered clusters, the gyrotropy of constituent particles manifests in the optical response.

B. Circular dichroism

The extinction cross section σ_T , the scattering cross section σ_S , and the absorption cross section σ_A of a cluster are [31]

$$\begin{aligned} \sigma_T &= -\frac{1}{k^2} \text{Re} \left[\sum_{plm} W_{lm}^{(p)*}(\hat{\mathbf{u}}_I, \hat{\mathbf{k}}_I) A_{lm}^{(p)}(\hat{\mathbf{u}}_I, \hat{\mathbf{k}}_I) \right], \\ \sigma_S &= \frac{1}{k^2} \sum_{plm} A_{lm}^{(p)}(\hat{\mathbf{u}}_I, \hat{\mathbf{k}}_I) A_{lm}^{(p)*}(\hat{\mathbf{u}}_I, \hat{\mathbf{k}}_I), \\ \sigma_A &= \sigma_T - \sigma_S. \end{aligned} \quad (35)$$

For a cluster of N particles, we use the geometrical cross section πNa^2 as a natural unit of area. We first assume that $\hat{\mathbf{k}}_I \parallel \hat{\mathbf{z}}$, i.e., the incident wave propagates along the gyration vector. We consider the absorption cross sections σ_+ and σ_- corresponding to the polarization vectors $\hat{\mathbf{u}}_{I1} = (\hat{\mathbf{x}} + i\hat{\mathbf{y}})/\sqrt{2}$ and $\hat{\mathbf{u}}_{I2} = (\hat{\mathbf{x}} - i\hat{\mathbf{y}})/\sqrt{2}$, respectively. $\hat{\mathbf{u}}_{I1}$ and $\hat{\mathbf{u}}_{I2}$ describe the left and right circularly polarized light, respectively. The circular dichroism of the system is $\sigma_{\text{CD}} = \sigma_+ - \sigma_-$.

Figure 5 shows $\sigma_{\text{CD}}/(\pi Na^2)$ for a monomer, dimer, and octamer of Bi:YIG nanoparticles. Here $a = d = 50$ nm. The overall behavior of the scaled dichroism spectra are the same. In particular, for $570 < \lambda < 600$ nm we find that $\sigma_{\text{CD}}/(\pi Na^2)$ is about 0.002. However, the spectra are distinguishable from each other. Indeed $\sigma_{\text{CD}}/(\pi Na^2)$ of a monomer (dimer, octamer) reaches its minimum -0.0482 (-0.055 , -0.0593) at wavelength 365 (365, 376) nm and gains its maximum 0.0583 (0.0625, 0.0757) at wavelength 460 (461, 463) nm.

We also studied the case $\hat{\mathbf{k}}_I \parallel \hat{\mathbf{y}}$ and find that σ_{CD} of monomer, dimer, and octamer are zero. This shows that the circular dichroism depends on the directions of the gyration vector and light wave vector with respect to the cluster axis.

IV. REMARKS

A few remarks are in order.

(i) We have assumed that the gyration vectors of all nanoparticles are parallel. This is not out of reach. Indeed using a sol-gel process, γ -Fe₂O₃ nanoparticle-doped silica matrix is obtained [7]. Noting that the magnetic nanoparticles are intrinsically anisotropic, a magnetic field is applied during the gelation process to orient the nanoparticles. After the gelation, nanoparticles stay locked in the matrix. Here one expects almost all nanoparticles to have the same optical orientation.

(ii) Linear clusters depicted in Fig. 1 deserve attention: A ferrofluid consisting of Fe₃O₄ nanoparticles dispersed in a hydrocarbon carrier exhibits terahertz Faraday rotation. In the absence of an external magnetic field, the nanoparticles are randomly distributed. A magnetic field triggers the particles to form chainlike clusters along the field direction [35].

(iii) For applications in integrated optics, one can envisage constructing a Faraday rotator by doping Bi:YIG nanoparticles in a *small* part of the waveguide. Intuitively, one expects the particles to spread randomly in the host material. Since the penetration depths of the particles are almost the same, a planar disordered cluster of particles may serve as a primitive model. Here we have shown that a cluster of 64 Bi:YIG particles exhibits considerable Faraday activity. Hence, in practice, only a small part of the waveguide must be lightly doped.

(iv) We perform multipole expansion of the fields up to a multipole order l_{\max} . We choose $6 \leq l_{\max} \leq 10$ to guarantee the numerical stability of our calculations. Note that the dipole approximation $l_{\max} = 1$ may reveal salient features of the optical response of small particles if $d > 3a$.

(v) Relying on the dipole approximation, the Faraday rotation spectrum of nanoparticle aggregates is studied [24]. It is shown that *analytical* expressions for $\chi - \psi$ and β of a dimer can be approximated as sinusoidal functions of 2ψ . For nanoparticles positioned on a helix, and a three-dimensional random gas of nanoparticles, a similar numerical result is obtained. Here we consider clusters with $d < a$, where the multipole interactions between nanoparticles are strong. Nevertheless, we observe that $\chi - \psi$ and β are almost sinusoidal functions of 2ψ .

(vi) For some parameters d, a, ω , etc., $\chi - \psi$ and β are nonsinusoidal functions of 2ψ [see, for example, Fig. 3(e) for wavelengths 365 and 400 nm]. However, still one can use the well-defined quantities [24]

$$\begin{aligned}\bar{\chi}_{\text{gyro}} &= \frac{1}{\pi} \int_0^\pi (\chi - \psi) d\psi, \\ \bar{\beta}_{\text{gyro}} &= \frac{1}{\pi} \int_0^\pi \beta d\psi,\end{aligned}\quad (36)$$

to distinguish nanoparticle aggregates of different magneto-optical activity.

(vii) In the limit $\epsilon_k = 0$, our theory describes light scattering from an aggregate of uniaxial anisotropic nanoparticles. The effect of anisotropy ratio ϵ_r on the scattering cross section of *one* particle is pronounced [36]. Thus the optical properties of an aggregate are expected to depend on the anisotropy ratio ϵ_r .

(viii) From a geometrical point of view, a cluster of nanoparticles is anisotropic to some extent. One can quantify

anisotropy of a set of points through various geometrical measures. For example, one can calculate the moment-of-inertia tensor $I_{\alpha,\beta} = \sum_{i=1}^N \delta_{\alpha,\beta} \mathbf{r}_i \cdot \mathbf{r}_i - (\mathbf{r}_i)_\alpha (\mathbf{r}_i)_\beta$ and its three real eigenvalues $I_1 \leq I_2 \leq I_3$. $I_1/(I_1 + I_2 + I_3)$ and $I_2/(I_1 + I_2 + I_3)$ may quantify anisotropy. From an optical point of view, not only the positions of the particles but also parameters such as a, ω , and ϵ_r influence the interaction of light and cluster. Here we suggest well-defined quantities

$$\begin{aligned}\bar{\chi}_{\text{aniso,s}} &= \frac{2}{\pi} \int_0^\pi (\chi - \psi) \sin(2\psi) d\psi, \\ \bar{\chi}_{\text{aniso,c}} &= \frac{2}{\pi} \int_0^\pi (\chi - \psi) \cos(2\psi) d\psi, \\ \bar{\beta}_{\text{aniso,s}} &= \frac{2}{\pi} \int_0^\pi \beta \sin(2\psi) d\psi, \\ \bar{\beta}_{\text{aniso,c}} &= \frac{2}{\pi} \int_0^\pi \beta \cos(2\psi) d\psi,\end{aligned}\quad (37)$$

to distinguish nanoparticle aggregates of different optical anisotropy.

(ix) We mentioned that the anisotropy of the cluster contributes to the polarization azimuth rotation $\chi - \psi$ and the ellipticity angle variation β . But one must notice that a cluster of nongyrotropic particles does not lead to a *nonreciprocal effect* such as the Faraday rotation. Indeed the time-reversal symmetry breaking is due to the presence of the (saturating) magnetic field that induces gyrotropy in the particles.

(x) Through a wise choice of the geometry, a set of spherical scatterers may approximate a nonspherical scatterer. Thus our multiparticle Mie theory can be used immediately to study the magneto-optical response of a nonspherical particle.

We have considered clusters composed of 64 Bi:YIG nanoparticles. For an ordered linear cluster, we find that $\chi - \psi = \chi_{\text{gyro}}$ and $\beta = \beta_{\text{gyro}}$ when light wave vector, gyration vector, and cluster axis are parallel [see Figs. 3(a) and 3(b)]. Here χ_{gyro} and β_{gyro} are about $\pm 0.5^\circ$. For planar rectangular and disordered clusters, we observe that expression (1) works well in a large domain of parameter space. $\chi - \psi$ and β of a *disordered* cluster may be larger than that of a rectangular cluster [see Figs. 3(c)–3(f)]. This considerably simplifies the design of small polarization rotators. Indeed at wavelength 485 nm, polarization rotations about $\pm 4^\circ$ are achievable [see Fig. 3(e)].

Our work can be extended in other directions: We assumed that all particles have the same radius, but the size polydispersity is expected to influence the Faraday rotation as well as the absorption spectrum [37]. Clusters of core-shell magnetoplasmonic particles are of immediate interest. Dichroism of two- and three-dimensional arrangements of gyrotropic particles deserves another study [25,38,39]. Many studies are devoted to light propagation in turbid media. It is known that Faraday rotation destroys coherent backscattering [40,41]. To further investigate this phenomenon, our multiparticle Mie theory is of use.

APPENDIX A: VECTOR MULTIPOLE FIELDS

The vector function $\mathbf{X}_{lm} = [l(l+1)]^{-1/2} \mathbf{L}Y_{lm}$, where the spherical harmonic Y_{lm} is the simultaneous eigenfunction

of the angular momentum operators \mathbf{L}^2 and L_z . It is convenient to introduce transverse vector harmonics $\mathbf{Z}_{lm}^{(1)}(\hat{\mathbf{k}}) = \mathbf{X}_{lm}(\hat{\mathbf{k}})$ and $\mathbf{Z}_{lm}^{(2)}(\hat{\mathbf{k}}) = \mathbf{X}_{lm}(\hat{\mathbf{k}}) \times \hat{\mathbf{k}}$. The vector multipole fields are solutions of the Maxwell equations that are eigenvectors of \mathbf{L}^2 and L_z :

$$\mathbf{L}_{lm}(\mathbf{r}, k) = \frac{1}{k} \nabla [j_l(kr) Y_{lm}],$$

$$\mathbf{J}_{lm}^{(1)}(\mathbf{r}, k) = j_l(kr) \mathbf{X}_{lm}(\hat{\mathbf{r}}),$$

$$\mathbf{J}_{lm}^{(2)}(\mathbf{r}, k) = \frac{1}{k} \nabla \times \mathbf{J}_{lm}^{(1)}(\mathbf{r}, k),$$

$$\mathbf{H}_{lm}^{(1)}(\mathbf{r}, k) = h_l(kr) \mathbf{X}_{lm}(\hat{\mathbf{r}}),$$

$$\mathbf{H}_{lm}^{(2)}(\mathbf{r}, k) = \frac{1}{k} \nabla \times \mathbf{H}_{lm}^{(1)}(\mathbf{r}, k), \tag{A1}$$

where j_l and h_l are spherical Bessel and spherical Hankel functions of the first kind, respectively [31].

We represent the vector multipole fields as

$$\begin{aligned} \mathbf{L}_{lm} = & \left[\sqrt{\frac{(l+m)(l-m)}{(2l-1)(2l+1)}} Y_{l-1,m} j_{l-1}(kr) - \sqrt{\frac{(l+m+1)(l-m+1)}{(2l+1)(2l+3)}} Y_{l+1,m} j_{l+1}(kr) \right] \xi_0 \\ & + \left[\sqrt{\frac{(l+m+2)(l+m+1)}{2(2l+1)(2l+3)}} Y_{l+1,m+1} j_{l+1}(kr) + \sqrt{\frac{(l-m)(l-m-1)}{2(2l-1)(2l+1)}} Y_{l-1,m+1} j_{l-1}(kr) \right] \xi_{-1} \\ & + \left[\sqrt{\frac{(l-m+2)(l-m+1)}{2(2l+1)(2l+3)}} Y_{l+1,m-1} j_{l+1}(kr) + \sqrt{\frac{(l+m)(l+m-1)}{2(2l-1)(2l+1)}} Y_{l-1,m-1} j_{l-1}(kr) \right] \xi_{+1}, \end{aligned} \tag{A2}$$

$$\mathbf{J}_{lm}^{(1)} = \frac{j_l(kr)}{\sqrt{l(l+1)}} \left[m Y_{lm} \xi_0 + \sqrt{\frac{(l-m)(l+1+m)}{2}} Y_{l,m+1} \xi_{-1} - \sqrt{\frac{(l+m)(l+1-m)}{2}} Y_{l,m-1} \xi_{+1} \right], \tag{A3}$$

$$\begin{aligned} \mathbf{J}_{lm}^{(2)} = & i \sqrt{\frac{l}{l+1}} \left[\sqrt{\frac{(l+m+1)(l-m+1)}{(2l+1)(2l+3)}} Y_{l+1,m} j_{l+1} + \frac{l+1}{l} \sqrt{\frac{(l+m)(l-m)}{(2l+1)(2l-1)}} Y_{l-1,m} j_{l-1} \right] \xi_0 \\ & + i \sqrt{\frac{l}{l+1}} \left[-\sqrt{\frac{(l+m+2)(l+m+1)}{2(2l+1)(2l+3)}} Y_{l+1,m+1} j_{l+1} + \frac{l+1}{l} \sqrt{\frac{(l-m)(l-m-1)}{2(2l-1)(2l+1)}} Y_{l-1,m+1} j_{l-1} \right] \xi_{-1} \\ & + i \sqrt{\frac{l}{l+1}} \left[-\sqrt{\frac{(l-m+2)(l-m+1)}{2(2l+1)(2l+3)}} Y_{l+1,m-1} j_{l+1} + \frac{l+1}{l} \sqrt{\frac{(l+m)(l+m-1)}{2(2l+1)(2l-1)}} Y_{l-1,m-1} j_{l-1} \right] \xi_{+1}, \end{aligned} \tag{A4}$$

where $\xi_{\pm 1} = \mp \frac{1}{\sqrt{2}}(\hat{e}_x \pm i \hat{e}_y)$ and $\xi_0 = \hat{e}_z$ are spherical basis vectors.

The following identities are of great use:

$$\begin{aligned} \nabla \cdot \mathbf{J}_{lm}^{(p)}(\mathbf{r}, k) &= \nabla \times \mathbf{L}_{lm}(\mathbf{r}, k) = 0, \\ \frac{1}{k} \nabla \times \mathbf{J}_{lm}^{(1)}(\mathbf{r}, k) &= \mathbf{J}_{lm}^{(2)}(\mathbf{r}, k), \\ \frac{1}{k} \nabla \times \mathbf{J}_{lm}^{(2)}(\mathbf{r}, k) &= \mathbf{J}_{lm}^{(1)}(\mathbf{r}, k). \end{aligned} \tag{A5}$$

We repeatedly encounter these integrals:

$$\begin{aligned} \int \mathbf{L}_{lm} \cdot \mathbf{L}_{l'm'}^* d\Omega &= [l j_{l-1}^2(kr) + (l+1) j_{l+1}^2(kr)] \frac{\delta_{ll'} \delta_{mm'}}{2l+1}, \\ \int \mathbf{J}_{lm}^{(1)} \cdot \mathbf{J}_{l'm'}^{(1)*} d\Omega &= j_l^2(kr) \delta_{ll'} \delta_{mm'}, \\ \int \mathbf{J}_{lm}^{(2)} \cdot \mathbf{J}_{l'm'}^{(2)*} d\Omega &= [(l+1) j_{l-1}^2(kr) + l j_{l+1}^2(kr)] \frac{\delta_{ll'} \delta_{mm'}}{2l+1}, \\ \int \mathbf{J}_{lm}^{(2)} \cdot \mathbf{L}_{l'm'}^* d\Omega &= [j_{l-1}^2(kr) - j_{l+1}^2(kr)] \frac{i \sqrt{l(l+1)} \delta_{ll'} \delta_{mm'}}{2l+1}, \\ \int \mathbf{L}_{lm} \cdot \mathbf{J}_{l'm'}^{(1)*} d\Omega &= 0. \end{aligned} \tag{A6}$$

To derive boundary conditions (22)–(25), we use the following integrals:

$$\begin{aligned} \int \mathbf{Z}_{l'm'}^{(p')} \cdot \mathbf{Z}_{l'm'}^{(p)*} d\Omega &= \delta_{pp'} \delta_{ll'} \delta_{mm'}, \\ \int \mathbf{J}_{lm}^{(1)} \cdot \mathbf{Z}_{l'm'}^{(1)*} d\Omega &= j_l(kr) \delta_{ll'} \delta_{mm'}, \\ \int \mathbf{J}_{lm}^{(1)} \cdot \mathbf{Z}_{l'm'}^{(2)*} d\Omega &= 0, \\ \int \mathbf{J}_{lm}^{(2)} \cdot \mathbf{Z}_{l'm'}^{(1)*} d\Omega &= 0, \\ \int \mathbf{J}_{lm}^{(2)} \cdot \mathbf{Z}_{l'm'}^{(2)*} d\Omega &= -\frac{1}{kr} [kr j_l(kr)]' \delta_{ll'} \delta_{mm'}, \\ \int \mathbf{L}_{lm} \cdot \mathbf{Z}_{l'm'}^{(1)*} d\Omega &= 0, \\ \int \mathbf{L}_{00} \cdot \mathbf{Z}_{l'm'}^{(2)*} d\Omega &= 0, \\ \int \mathbf{L}_{lm} \cdot \mathbf{Z}_{l'm'}^{(2)*} d\Omega &= \frac{i \sqrt{l(l+1)}}{kr} j_l(kr) \delta_{ll'} \delta_{mm'}. \end{aligned} \tag{A7}$$

APPENDIX B: COEFFICIENTS \tilde{g}_{qp}^{lm} , \tilde{e}_{qp}^{lm} , \tilde{f}_{qp}^{lm} , \tilde{g}_{qp}^{lm} , \tilde{e}_{qp}^{lm} , AND \tilde{f}_{qp}^{lm}

The inverse of the permittivity tensor (2) is

$$\begin{aligned} \epsilon_z \overset{\leftrightarrow}{\epsilon}_g^{-1} &= \begin{pmatrix} \epsilon'_r & -i\epsilon'_k & 0 \\ i\epsilon'_k & \epsilon'_r & 0 \\ 0 & 0 & 1 \end{pmatrix}, \\ &= (\epsilon'_k - \epsilon'_r)\xi_{-1}\xi_{+1} - (\epsilon'_r + \epsilon'_k)\xi_{+1}\xi_{-1} + \xi_0\xi_0, \end{aligned} \quad (\text{B1})$$

where $\epsilon'_r = \epsilon_r/(\epsilon_r^2 - \epsilon_k^2)$ and $\epsilon'_k = -\epsilon_k/(\epsilon_r^2 - \epsilon_k^2)$. The explicit expressions (A3) and (B1) allow us to write

$$\epsilon_z \overset{\leftrightarrow}{\epsilon}_g^{-1} \cdot \mathbf{J}_{lm}^{(1)} = \frac{j_l(kr)}{\sqrt{l(l+1)}} \left[m Y_{lm} \xi_0 - \sqrt{\frac{(l-m)(l+1+m)}{2}} (\epsilon'_k - \epsilon'_r) Y_{l,m+1} \xi_{-1} - \sqrt{\frac{(l+m)(l+1-m)}{2}} (\epsilon'_r + \epsilon'_k) Y_{l,m-1} \xi_{+1} \right]. \quad (\text{B2})$$

Now using Eqs. (A3) and (B2) and $\xi_\mu \cdot \xi_{\mu'}^* = (-1)^{\mu'} \xi_\mu \cdot \xi_{-\mu'} = \delta_{\mu\mu'}$, it is straightforward to obtain $\int [\epsilon_z \overset{\leftrightarrow}{\epsilon}_g^{-1} \cdot \mathbf{J}_{lm}^{(1)}] \cdot \mathbf{J}_{l'm'}^{(1)*} d\Omega$. Using Eqs. (9) and (A6) to calculate the same scalar, one finds

$$\tilde{g}_{l'm'}^{lm} = \frac{(l^2 + l - m^2)\epsilon'_r + m\epsilon'_k + m^2}{l(l+1)} \delta_{ll'} \delta_{mm'}. \quad (\text{B3})$$

Calculating $\int [\epsilon_z \overset{\leftrightarrow}{\epsilon}_g^{-1} \cdot \mathbf{J}_{lm}^{(1)}] \cdot \mathbf{L}_{l'm'}^* d\Omega$ and $\int [\epsilon_z \overset{\leftrightarrow}{\epsilon}_g^{-1} \cdot \mathbf{J}_{lm}^{(1)}] \cdot \mathbf{J}_{l'm'}^{(2)*} d\Omega$ using the equivalent expressions (9) and (B2), one finds

$$\begin{aligned} \tilde{e}_{l'm'}^{lm} a_0 + \tilde{f}_{l'm'}^{lm} b_0 &= A_0 j_{l'+1}^2(kr) \delta_{l,l'+1} \delta_{mm'} + B_0 j_{l'-1}^2(kr) \delta_{l,l'-1} \delta_{mm'}, \\ \tilde{e}_{l'm'}^{lm} c_0 + \tilde{f}_{l'm'}^{lm} d_0 &= i \sqrt{\frac{l'}{l'+1}} A_0 j_{l'+1}^2(kr) \delta_{l,l'+1} \delta_{mm'} - i \sqrt{\frac{l'+1}{l'}} B_0 j_{l'-1}^2(kr) \delta_{l,l'-1} \delta_{mm'}, \end{aligned}$$

where

$$\begin{aligned} a_0 &= \frac{i\sqrt{l'(l'+1)}}{(2l'+1)} [j_{l'-1}^2(kr) - j_{l'+1}^2(kr)], \quad b_0 = \frac{1}{(2l'+1)} [l' j_{l'-1}^2(kr) + (l'+1) j_{l'+1}^2(kr)], \\ c_0 &= \frac{1}{(2l'+1)} [(l'+1) j_{l'-1}^2(kr) + l' j_{l'+1}^2(kr)], \quad d_0 = \frac{-i\sqrt{l'(l'+1)}}{(2l'+1)} [j_{l'-1}^2(kr) - j_{l'+1}^2(kr)], \\ A_0 &= \sqrt{\frac{(l'+m'+1)(l'-m'+1)}{(l'+1)(l'+2)(2l'+1)(2l'+3)}} [m'(\epsilon'_r - 1) - (l'+2)\epsilon'_k], \quad B_0 = -\sqrt{\frac{l'^2 - m'^2}{l'(l'-1)(4l'^2 - 1)}} [m'(\epsilon'_r - 1) + (l'-1)\epsilon'_k]. \end{aligned}$$

The solution of the above set of equations is

$$\begin{aligned} \tilde{e}_{l'm'}^{lm} &= i \sqrt{\frac{(l-1)(l^2 - m^2)}{(l+1)(4l^2 - 1)}} \frac{[m(\epsilon'_r - 1) - (l+1)\epsilon'_k]}{l} \delta_{l-1,l'} \delta_{mm'} + i \sqrt{\frac{(l+2)[(l+1)^2 - m^2]}{l(2l+1)(2l+3)}} \frac{[m(\epsilon'_r - 1) + l\epsilon'_k]}{l+1} \delta_{l+1,l'} \delta_{mm'}, \\ \tilde{f}_{l'm'}^{lm} &= \sqrt{\frac{l^2 - m^2}{l(l+1)(4l^2 - 1)}} [m(\epsilon'_r - 1) - (l+1)\epsilon'_k] \delta_{l-1,l'} \delta_{mm'} - \sqrt{\frac{(l+1)^2 - m^2}{l(l+1)(2l+1)(2l+3)}} [m(\epsilon'_r - 1) + l\epsilon'_k] \delta_{l+1,l'} \delta_{mm'}. \end{aligned} \quad (\text{B4})$$

Following the same procedure, we obtain

$$\begin{aligned} \tilde{g}_{l'm'}^{lm} &= \frac{-i}{l+1} \sqrt{\frac{l[(l+1)^2 - m^2]}{(l+2)(2l+1)(2l+3)}} [m(\epsilon'_r - 1) - (l+2)\epsilon'_k] \delta_{l+1,l'} \delta_{mm'} - \frac{i}{l} \sqrt{\frac{(l+1)(l^2 - m^2)}{(l-1)(4l^2 - 1)}} [m(\epsilon'_r - 1) + (l-1)\epsilon'_k] \delta_{l-1,l'} \delta_{mm'}, \\ \tilde{e}_{l'm'}^{lm} &= \delta_{ll'} \delta_{mm'} + \frac{[(2l^2 + 2l + 3)m^2 + (2l^2 + 2l - 3)l(l+1)](\epsilon'_r - 1) + (4l^2 + 4l - 3)m\epsilon'_k}{l(l+1)(2l-1)(2l+3)} \delta_{ll'} \delta_{mm'} \\ &\quad - \sqrt{\frac{(l-2)(l+1)[(l-1)^2 - m^2](l^2 - m^2)}{(l-1)l(2l-3)(2l+1)}} \frac{\epsilon'_r - 1}{2l-1} \delta_{l-2,l'} \delta_{mm'} - \sqrt{\frac{l(l+3)[(l+1)^2 - m^2][(l+2)^2 - m^2]}{(l+1)(l+2)(2l+1)(2l+5)}} \frac{\epsilon'_r - 1}{2l+3} \delta_{l+2,l'} \delta_{mm'}, \\ \tilde{f}_{l'm'}^{lm} &= i \sqrt{\frac{(l+1)[(l-1)^2 - m^2](l^2 - m^2)}{l(2l-3)(2l+1)}} \frac{\epsilon'_r - 1}{2l-1} \delta_{l-2,l'} \delta_{mm'} - i \sqrt{\frac{l[(l+1)^2 - m^2][(l+2)^2 - m^2]}{(l+1)(2l+1)(2l+5)}} \frac{\epsilon'_r - 1}{2l+3} \delta_{l+2,l'} \delta_{mm'} \\ &\quad - i \frac{(l^2 + l - 3m^2)(\epsilon'_r - 1) - (2l-1)(2l+3)m\epsilon'_k}{\sqrt{l(l+1)(2l-1)(2l+3)}} \delta_{ll'} \delta_{mm'}. \end{aligned} \quad (\text{B5})$$

- [1] V. Antonov, B. Harmon, and A. Yaresko, *Electronic Structure and Magneto-Optical Properties of Solids* (Kluwer Academic, Dordrecht, Netherlands, 2004).
- [2] Š. Višňovský, *Optics in Magnetic Multilayers and Nanostructures* (Taylor & Francis, Boca Raton, FL, 2006).
- [3] A. K. Zvezdin and V. A. Kotov, *Modern Magneto-optics and Magneto-optical Materials* (IOP, Bristol, UK, 1997).
- [4] J. P. Castera and T. Suzuki, Magneto-optical devices, in *The Optics Encyclopedia: Basic Foundations and Practical Applications*, edited by T. G. Brown, K. Creath, H. Kogelnik, M. Kriss, J. Schmit, and M. J. Weber (Wiley-VCH, Weinheim, 2004).
- [5] H. Dötsch, N. Bahlmann, O. Zhuromskyy, M. Hammer, L. Wilkens, R. Gerhardt, and P. Hertel, Applications of magneto-optical waveguides in integrated optics: Review, *J. Opt. Soc. Am. B* **22**, 240 (2005).
- [6] D. A. Smith, Y. A. Barnakov, B. L. Scott, S. A. White, and K. L. Stokes, Magneto-optical spectra of closely spaced magnetite nanoparticles, *J. Appl. Phys.* **97**, 10M504 (2005).
- [7] F. Bentivegna, M. Nyvlt, J. Ferré, J. P. Jamet, A. Brun, Š. Višňovský, and R. Urban, Magnetically textured γ -Fe₂O₃ nanoparticles in a silica gel matrix: Optical and magneto-optical properties, *J. Appl. Phys.* **85**, 2270 (1999).
- [8] C. Clavero, A. Cebollada, G. Armelles, Y. Huttel, J. Arbiol, F. Peiró, and A. Cornet, Size effects in the magneto-optical response of Co nanoparticles, *Phys. Rev. B* **72**, 024441 (2005).
- [9] J. L. Menéndez, B. Bescós, G. Armelles, R. Serna, J. Gonzalo, R. Doole, A. K. Petford-Long, and M. I. Alonso, Optical and magneto-optical properties of Fe nanoparticles, *Phys. Rev. B* **65**, 205413 (2002).
- [10] I. S. Edelman, D. A. Petrov, R. D. Ivantsov, S. M. Zharkov, D. A. Velikanov, G. G. Gumarov, V. I. Nuzhdin, V. F. Valeev, and A. L. Stepanov, Study of morphology, magnetic properties, and visible magnetic circular dichroism of Ni nanoparticles synthesized in SiO₂ by ion implantation, *Phys. Rev. B* **87**, 115435 (2013).
- [11] T. Y. Kim, T. Hirano, Y. Yamazaki, and Y. D. Hong, Transmission electron microscopy estimation of Bi-YIG nanoparticle hybridized with plastic material, *J. Appl. Phys.* **93**, 7501 (2003).
- [12] J. W. Lee, J. H. Oh, J. C. Lee, and S. C. Choi, Magneto-optical properties of Bi-YIG nanoparticles dispersed in the organic binder, *J. Magn. Magn. Mater.* **272**, 2230 (2004).
- [13] Y. J. Wu, R. Y. Hong, L. S. Wang, G. Q. Di, H. Z. Li, B. Xu, Y. Zheng, and D. G. Wei, Molten-salt synthesis and characterization of Bi-substituted yttrium garnet nanoparticles, *J. Alloys Compd.* **481**, 96 (2009).
- [14] B. Sepúlveda, J. B. González-Díaz, A. García-Martín, L. M. Lechuga, and G. Armelles, Plasmon-Induced Magneto-Optical Activity in Nanosized Gold Disks, *Phys. Rev. Lett.* **104**, 147401 (2010).
- [15] G. Armelles, A. Cebollada, A. García-Martín, and M. U. González, Magnetoplasmonics: Combining magnetic and plasmonic functionalities, *Adv. Opt. Mater.* **1**, 10 (2013).
- [16] P. Varytis, N. Stefanou, A. Christofi, and N. Papanikolaou, Strong circular dichroism of core-shell magnetoplasmonic nanoparticles, *J. Opt. Soc. Am. B* **32**, 1063 (2015).
- [17] L. Wang, K. Yang, C. Clavero, A. J. Nelson, K. J. Carroll, E. E. Carpenter, and R. A. Lukaszew, Localized surface plasmon resonance enhanced magneto-optical activity in core-shell Fe-Ag nanoparticles, *J. Appl. Phys.* **107**, 09B303 (2010).
- [18] P. K. Jain, Y. H. Xiao, R. Walsworth, and A. E. Cohen, Surface plasmon resonance enhanced magneto-optics (SuPREMO): Faraday rotation enhancement in gold-coated iron oxide nanocrystals, *Nano Lett.* **9**, 1644 (2009).
- [19] R. K. Dani, H. Wang, S. H. Bossmann, G. Wysin, and V. Chikan, Faraday rotation enhancement of gold coated Fe₂O₃ nanoparticles: Comparison of experiment and theory, *J. Chem. Phys.* **135**, 224502 (2011).
- [20] Y. Li, Q. Zhang, A. V. Nurmikko, and S. Sun, Enhanced magneto-optical response in dumbbell-like Ag-CoFe₂O₄ nanoparticle pairs, *Nano Lett.* **5**, 1689 (2005).
- [21] J. L. W. Li and W. L. Ong, A new solution for characterizing electromagnetic scattering by a gyroelectric sphere, *IEEE Trans. Antennas Propag.* **59**, 3370 (2011).
- [22] J. L. W. Li, W. L. Ong, and K. H. R. Zheng, Anisotropic scattering effects of a gyrotropic sphere characterized using the T-matrix method, *Phys. Rev. E* **85**, 036601 (2012).
- [23] J. J. Wang, Y. P. Han, L. Han, and Z. W. Cui, Electromagnetic scattering from gyroelectric anisotropic particle by the T-matrix method, *J. Quant. Spectrosc. Radiat. Transfer* **135**, 20 (2014).
- [24] S. Pakdel and M. F. Miri, Faraday rotation and circular dichroism spectra of gold and silver nanoparticle aggregates, *Phys. Rev. B* **86**, 235445 (2012).
- [25] A. Mohammadzadeh and M. F. Miri, Magnetic linear and circular dichroism of planar sets of hollow silver nanoparticles: Engineering the spectra by hollow size, *J. Opt. Soc. Am. B* **33**, 711 (2016).
- [26] A. Christofi and N. Stefanou, Nonreciprocal optical response of helical periodic structures of plasma spheres in a static magnetic field, *Phys. Rev. B* **87**, 115125 (2013).
- [27] A. Christofi and N. Stefanou, Nonreciprocal photonic surface states in periodic structures of magnetized plasma nanospheres, *Phys. Rev. B* **88**, 125133 (2013).
- [28] A. Christofi and N. Stefanou, Layer multiple scattering calculations for nonreciprocal photonic structures, *Int. J. Mod. Phys. B* **28**, 1441012 (2014).
- [29] P. Varytis, P. A. Pantazopoulos, and N. Stefanou, Enhanced Faraday rotation by crystals of core-shell magnetoplasmonic nanoparticles, *Phys. Rev. B* **93**, 214423 (2016).
- [30] E. Almpanis, P. A. Pantazopoulos, N. Papanikolaou, V. Yannopoulos, and N. Stefanou, Metal-nanoparticle arrays on a magnetic garnet film for tunable plasmon-enhanced Faraday rotation, *J. Opt. Soc. Am. B* **33**, 2609 (2016).
- [31] F. Borghese, P. Denti, and R. Saija, *Scattering from Model Nonspherical Particles* (Springer, Berlin, 2007).
- [32] Y. P. Svirko and N. I. Zheludev, *Polarization of Light in Nonlinear Optics* (Wiley, Chichester, UK, 1998).
- [33] V. Doormann, J. P. Krumme, and H. Lenz, Optical and magneto-optical tensor spectra of bismuth-substituted yttrium-iron-garnet films, *J. Appl. Phys.* **68**, 3544 (1990).
- [34] E. Collett, *Polarized Light: Fundamentals and Applications* (Marcel Dekker, New York, 1993).
- [35] M. Shalaby, M. Peccianti, Y. Ozturk, M. Clerici, I. Al-Naib, L. Razzari, T. Ozaki, A. Mazhorova, M. Skorobogatiy, and R. Morandotti, Terahertz Faraday rotation in a magnetic liquid: High magneto-optical figure of merit and broadband operation in a ferrofluid, *Appl. Phys. Lett.* **100**, 241107 (2012).
- [36] C. W. Qiu, L. Gao, J. D. Joannopoulos, and M. Soljačić, Light scattering from anisotropic particles: Propagation,

- localization, and nonlinearity, *Laser Photon. Rev.* **4**, 268 (2010).
- [37] Z. Naeimi and M. F. Miri, Optical properties of fractal aggregates of nanoparticles: Effects of particle size polydispersity, *Phys. Rev. B* **80**, 224202 (2009).
- [38] V. Yannopapas, Circular dichroism in planar nonchiral plasmonic metamaterials, *Opt. Lett.* **34**, 632 (2009).
- [39] S. Droulias and V. Yannopapas, Broad-band giant circular dichroism in metamaterials of twisted chains of metallic nanoparticles, *J. Phys. Chem. C* **117**, 1130 (2013).
- [40] D. Lacoste and B. A. van Tiggelen, Coherent backscattering of light in a magnetic field, *Phys. Rev. E* **61**, 4556 (2000).
- [41] L. Schertel, G. J. Aubry, C. M. Aegerter, and G. Maret, Coherent multiple light scattering in Faraday active materials, *Eur. Phys. J. Spec. Top.* **226**, 1409 (2017).